Technology Assessment

Liver intravoxel incoherent motion (IVIM) magnetic resonance imaging: a comprehensive review of published data on normal values and applications for fibrosis and tumor evaluation

Yáo T. Li[1], Jean-Pierre Cercueil[2], Jing Yuan[3], Weitian Chen[1], Romaric Loffroy[2], Yì Xiáng J. Wáng[1]

[1]Department of Imaging and Interventional Radiology, Faculty of Medicine, The Chinese University of Hong Kong, Prince of Wales Hospital, New Territories, Hong Kong SAR, China; [2]Department of Vascular and Interventional Radiology, François-Mitterrand Teaching Hospital, University of Burgundy, Dijon, France; [3]Medical Physics and Research Department, Hong Kong Sanatorium & Hospital, Happy Valley, Hong Kong SAR, China

Correspondence to: Dr. Yì Xiáng J. Wáng. Department of Imaging and Interventional Radiology, Faculty of Medicine, The Chinese University of Hong Kong, Prince of Wales Hospital, New Territories, Hong Kong SAR, China. Email: yixiang_wang@cuhk.edu.hk.

Abstract: A comprehensive literature review was performed on liver intravoxel incoherent motion (IVIM) magnetic resonance imaging (MRI) technique and its applications. Heterogeneous data have been reported. IVIM parameters are magnetic field strength dependent to a mild extent. A lower Dslow (D) value at 3 T than at 1.5 T and higher perfusion fraction (PF) value at 3 T than at 1.5 T were noted. An increased number of b values are associated with increased IVIM parameter measurement accuracy. With the current status of art, IVIM technique is not yet capable of detecting early stage liver fibrosis and diagnosing liver fibrosis grades, nor can it differentiate liver tumors. Though IVIM parameters show promise for tumor treatment monitoring, till now how PF and Dfast (D*) add diagnostic value to Dslow or apparent diffusion coefficient (ADC) remains unclear. This paper shows the state-of-art IVIM MR technique is still not able to offer reliable measurement for liver. More works on the measurement robustness are warranted as they are essential to justify follow-up clinical studies on patients.

Keywords: Magnetic resonance imaging (MRI); intravoxel incoherent motion (IVIM); diffusion; perfusion; liver; fibrosis; tumour

Submitted Jan 01, 2017. Accepted for publication Jan 14, 2017.
doi: 10.21037/qims.2017.02.03
View this article at: http://dx.doi.org/10.21037/qims.2017.02.03

Introduction and basic principles of intravoxel incoherent motion (IVIM)

Diffusion weighted (DW)-magnetic resonance imaging (MRI) is sensitive to the thermally driven random motion of water protons, which is modified in tissues by their interactions with cell membranes and macromolecules. In the presence of a magnetic field gradient, diffusion of water molecules causes a phase dispersion of the transverse magnetization, which results in the attenuation of the MRI signal (1). Initially, the diffusion effect was described by a mono-exponential decay model (2). However, perfusion can contribute to the diffusion measurements significantly because of the incoherent motion of blood in pseudorandom capillary network at the macroscopic level (1,3-5). Thus, diffusion coefficient of water in tissues reflects tissue cellularity, the tortuosity of the extracellular space, integrity of cell membranes, and viscosity of fluids. IVIM reflects the random microscopic motion that occurs in voxels on MR images of water molecules (either intra-cellular or extracellular) and the microcirculation of blood. In 1986, Le Bihan *et al.* (1,3) proposed the principle of IVIM which enables the quantitative parameters that separately reflect tissue diffusivity and tissue microcapillary perfusion to be estimated. IVIM signal attenuation is modeled according to

the equation

$$SI(b) = SI_0[(1-PF)\cdot\exp^{(-b\cdot Dslow)} + PF\cdot\exp^{(-b\cdot Dfast)}] \quad [1]$$

where SI(b) and SI_0 denote the signal intensity acquired with the b-factor value of b and b =0 s/mm^2, respectively. Perfusion fraction (PF) is the fraction of the pseudo-diffusion linked to microcirculation, Dslow (or D) is the true diffusion coefficient representing the pure molecular diffusion (slow component of diffusion), and Dfast (D*) is the pseudo-diffusion coefficient representing the incoherent microcirculation within the voxel (perfusion-related diffusion, or fast component of diffusion). According to IVIM theory, diffusion and perfusion are affected by several tissue characteristics, including the presence of restrictive barriers within tissue, the viscosity of the fluid in which the spins are diffusing, and the velocity and fractional volume of perfusing spins (6). These characteristics may enable IVIM MRI to detect and characterize the tissue changes caused by diseases.

Previously, the use of IVIM imaging was limited to neuroradiologic applications because the abdominal organs can be subject to respiratory and other motion artifacts. The advent of respiratory gating combined with parallel imaging allows IVIM MRI to be attempted in the evaluation of abdominal organs, such as liver (7-12). Yamada *et al.* (7) were the first to assess IVIM MRI in abdominal organs, although they used only limited number of b values (30, 300, 900, and 1,100 s/mm^2), and did not calculate pseudo-diffusion values. Recently there are greater interests of using IVIM technique to study diffused liver diseases such as liver fibrosis and nonalcoholic fatty liver disease; to detect and characterize liver tumor; and to evaluate treatment response.

A prerequisite to translating the growing interest in IVIM imaging into clinical applications is its accurate measurement of normative value of IVIM parameters and acceptable reproducibility across different clinical settings (13,14). Nevertheless, accurate IVIM quantification is challenging, partially due to the limited sampling and low signal-to-noise ratio (SNR) for fast data acquisition of the liver (15-17). Even in the brain, where there is almost no motion effect, the cross-center agreement has been recently shown to be sub-optimal. The recent study of Grech-Sollars *et al.* (13) demonstrated that compared with apparent diffusion coefficient (ADC) and diffusion tensor imaging (DTI) parameters, the IVIM parameter PF had a high intra-scanner coefficient of variation (CoV) of 8.4% and inter-scanner CoV of 24.8%. Till now, the actual values of PF and Dfast remain unclear, and the optimal clinical settings for IVIM imaging are still under debate. This study aims to review the mean values and variability of Dslow, PF and Dfast of liver in the published literatures, and understand how the data acquisition set-up may impact the measurement of these values.

IVIM parameters of healthy liver in published literatures

We performed literature search using the PubMed searching tool (https://www.ncbi.nlm.nih.gov/pubmed) on September 26, 2016. The search word combination was "(Intravoxel Incoherent Motion OR IVIM) AND liver". This search generated 28 titles for human study of normal liver parenchyma and four titles for animal study (*Figure 1*).

The results of reported PF, Dslow and Dfast value were shown in *Tables 1,2* with frequency distribution and scatter plot shown in *Figure 2*. One study (18) was excluded due to unreasonable PF values of 369.14%±31.50%, as by definition PF has to be less than 100%. The results show Dslow is the most reliable parameter among the three parameters, with the mean and medium being both 1.09 ×10^{-3} mm^2/s. However, among the published studies, considerable variation still exists, with a CoV of 0.16. The measurement of PF showed a considerable variability, with a median value of 22.40% and a CoV of 0.37. Liver receives a total blood flow of 100–130 mL/min per 100 g liver in man, and of this 25–30% is supplied by the hepatic artery and the remainder by the portal vein (25-29). It is estimated that hepatic artery accounts for 1%, portal vein for 5%, hepatic vein for 5%, and small-vessel content for 14% of blood flow (25,29-32). In addition, blood volume account for 1/3 water content in liver (25). According to IVIM, PF is defined as partial volume of the whole capillary vascular fraction. PF can be estimated by multiplying the percentage of blood taking account for water (1/3) by the percentage of capillary blood taking account for total hepatic blood volume (14%/25%=56%), which is estimated to be around 18% (25).

Lemke *et al.* (33) demonstrated that overestimation of PF is dependent on echo time. To simplify the reasoning Lemke considered only the T2 effect. The longer the echo time, the greater the signal decays at low b values, which indicates the increase of estimated PF. This phenomenon is due to the faster transverse relaxation of the tissue compartment signal (i.e., the liver), which increases the signal fraction of

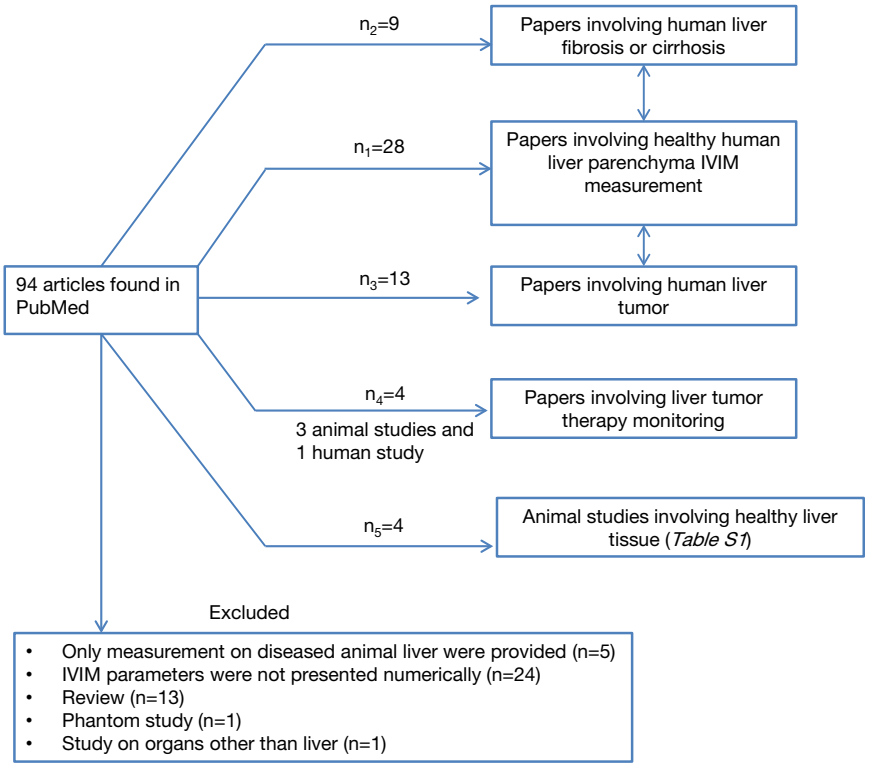

Figure 1 Flow diagram of literature selection. The result from four animal studies is shown in the *Table S1*.

Table 1 Results of reported PF, Dslow and Dfast values*

Results	Dslow ($\times 10^{-3}$ mm^2/s)	PF (%)	Dfast ($\times 10^{-3}$ mm^2/s)
Median	1.09	22.40	70.60
Range	0.66–1.50	5.50–47.07	13.60–136.00
Mid 50% data distribution**	1.005–1.163	17.70–28.00	44.00–91.99
Mean	1.09	23.05	70.02
SD	0.17	8.48	31.01
CoV	0.16	0.37	0.44

*, data of Chen *et al*. (18) were excluded as outlier because of extreme large PF value (369.14±31.50%). According to IVIM principle, PF should be presented as percentage and range from 0% to 100%, unreasonable large PF value indicates erroneous IVIM fitting process; **, mid 50% data distribution: middle two quartiles; PF, perfusion fraction; SD, standard deviation; CoV, coefficient of variation.

the vascular component. In addition, it is necessary to take into account of complexity of the signal in EPI sequence for IVIM acquisition, in particular the susceptibility effect. The effects of susceptibility are rather complex, which depend on the shift of phase during the reading. These shifts of phase in turn depend not only on the magnetic field but also on, among others, the K-space acquisition ordering mode, image resolution, acquisition segmentation, and receiver bandwidth. The iron (Fe^{+++}), mainly as intracellular deposits of ferritin, also influences DW signal and thus IVIM estimation. Hemochromatosis deposits are mainly in hepatocytes, while for hepatosiderosis the iron is mainly

Table 2 Summary of healthy liver IVIM studies with Dslow and PF value in the mid 50% data (middle two quartile) distribution of reported value

Paper	Subject number	PF (%)	Dslow (10^{-3} mm^2/s)	Dfast (10^{-3} mm^2/s)	Field strength (T)	Breath compensation	b value distribution (s/mm^2)	Post-processing algorithm
Leporq *et al.*, 2015 (19)	25	21.90±4.90	1.08±0.07	79.00±23.50	3.0	FB	0, 10, 80, 800	ROI analysis and nonlinear least-square fitting
Luciani *et al.*, 2008 (11)	25	27.00±5.30	1.10±0.70	79.10±18.10	1.5	Respiratory trigger	0, 10, 20, 30, 40, 50, 100, 200, 400, 800	Pixel-wise asymptotic fitting then ROI analysis with parametric maps
Taimouri *et al.*, 2015 (20)	29	25.00±18.00	1.01±0.29	54.60±55.10	1.5	FB	5, 50, 100, 200, 400, 600, 800	Pixel-wise asymptotic fitting then ROI analysis with parametric maps
Wurnig *et al.*, 2016 (21)	8	22.90	1.16	65.50	3.0	FB	0, 10, 20, 40, 90, 100, 170, 200, 210, 240, 390, 530, 620, 750, 970, 1000	ROI analysis and asymptotic fitting with parameter-free algorithm
Jerome *et al.*, 2014 (22)	10	17.70±2.90	1.16±0.12	44.00±5.00	1.5	FB	0, 20, 40, 60, 80, 100, 250, 500, 750	ROI analysis then Bayesian fitting
Lee *et al.*, 2015 (23)	12	22.00±4.00	1.00±0.07	116.71±100.20	1.5	Electrocardiography (ECG) triggering (ET)	0, 30, 60, 100, 150, 200, 400, 600, 900	Pixel-wise least-squares fitting then ROI analysis with parametric maps
Regini *et al.*, 2015 (24)	40	22.40±7.20	1.05±0.11	40.70±19.90	3.0	Respiratory trigger	0, 25, 50, 75, 100, 150, 200, 250, 300, 400, 500, 600, 700, 800	ROI analysis then asymptotic fitting

IVIM, intravoxel incoherent motion; PF, perfusion fraction, FB, free-breathing.

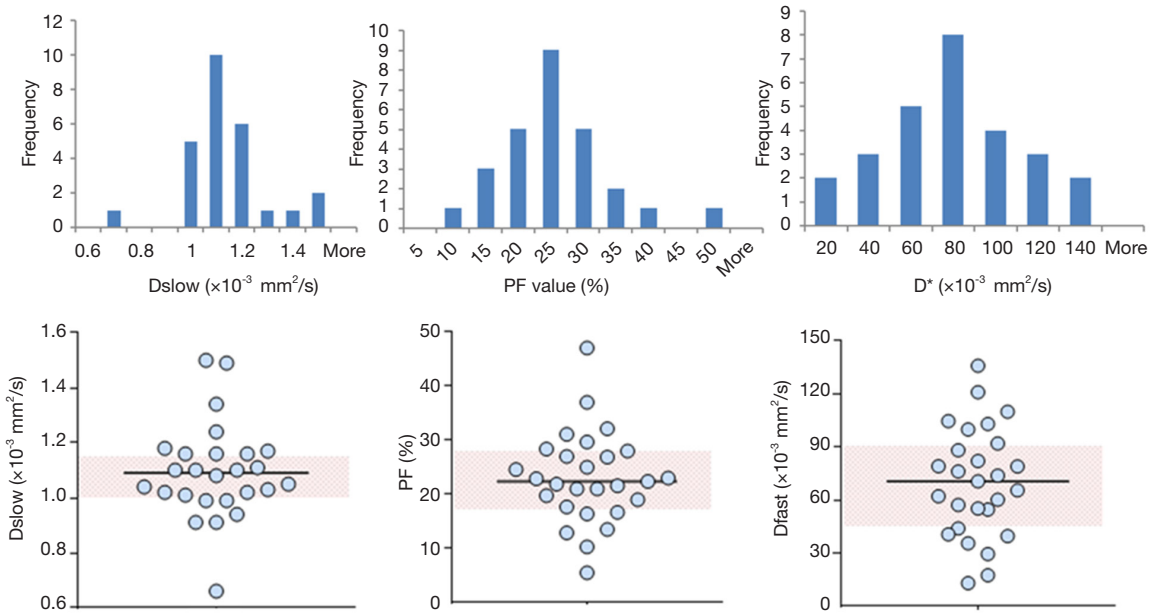

Figure 2 Histogram and scatter plot show the median value and distribution of Dslow (D), perfusion fraction (PF), and Dfast (D*) of healthy liver parenchyma reported in 27 studies. Dslow, PF, Dfast have a median value of 1.09 ×10^{-3} mm^2/s, 22.40%, 70.60×10^{-3} mm^2/s respectively. Pink shadow in scatter plot indicates mid 50% data distribution of reported value (middle two quartiles).

situated in the Kupfer, stellate and mesenchymal cells. This can partially explain the differences in the reported results according to the magnetic field or other acquisition's parameters (34-38).

With the 27 studies, Dfast has a mean value of 70.02 mm^2/s (median: 70.60 mm^2/s), and a high CoV of 0.44, which is the worst among the three parameters. Pekar *et al.* (39) commented that Dfast in particular tends to be unstable unless an unrealistically high SNR is achieved. It can be seen in *Figure 2* that while both Dslow and PF values tend to aggregate around the medium value, Dfast values remain scattered.

That Dslow has better reproducibility, PF has sub-optimal reproducibility and Dfast has the worse reproducibility has been demonstrated in individual publications. Andreou *et al.* (n=14) (17) reported 95% confidence intervals of percentage difference between the paired measurements for Dslow, PF, and Dfast of –5.12% to 8.09% (median: 1.0×$10^{-3}$$mm^2$/s), –24.3% to 25.1% (median: 18.6%) and –31.2% to 59.1% (median: 51.9× $10^{-3}$$mm^2$/s) respectively. Kakite *et al.* (n=11) (40) reported CoV of Dslow, PF, and Dfast of 13.2% (range, 1.2–28.5%), 25.3% (range, 9.3–84.9%), and 59.0% (range, 2.4–121.3%) respectively, and the Bland-Altman limits of agreement for Dslow, PF, and Dfast was –32.8% to 28.4%, –74.6% to 56.4%, and –151.2% to 132.7% respectively. It has been reported that IVIM parameter reproducibility also varies with tissue properties. Andreou *et al.* (17), Kakite *et al.* (40), ter Voert *et al.* (34) demonstrated that reproducibility of IVIM parameters was generally better in healthy liver parenchyma compared to liver tumors. Of note, ter Voert *et al.* (34) performed study with extensive b values (n=25), and reported a Dslow value of 0.83±0.18×10^{-3} mm^2/s, PF of 30±6.8%, and Dfast of 124.4±84.5×10^{-3} mm^2/s. Wurnig *et al.* (41) performed study with optimized b values (n=13) and reported the measured results of Dslow of 0.74±0.13×10^{-3} mm^2/s, PF of 22.6±7.4%, and Dfast of 88.7±42.5×10^{-3} mm^2/s for right liver lobe.

Patel *et al.* (12) and Hectors *et al.* (35) reported that there was no information overlap (or can be interpreted as poor correlation) between IVIM parameters and dynamic contrast enhanced (DCE) MRI metrics.

Factors influencing IVIM parameter measurement accuracy

Magnetic field strength

All the liver IVIM data included in this analysis were acquired at 1.5 or 3 T. For the reported 27 studies, median

value for Dslow is 1.11×10^{-3} mm^2/s (mean: 1.13×10^{-3} mm^2/s) and 1.02×10^{-3} mm^2/s (mean: 1.04×10^{-3} mm^2/s) for 1.5 and 3 T respectively (P=0.072); median value for PF is 22.00% (mean: 21.54%) and 22.65% (mean: 24.46%) for 1.5 and 3T respectively (P=0.512); and median value for Dfast is 67.01 (mean: 68.87) and 73.40×10^{-3} mm^2/s (mean: 73.46×10^{-3} mm^2/s) for 1.5 and 3T respectively (P=0.438) (*Table 3*). The results of *Figure 3* concur with the recent paper by Cui *et al*. (50). Cui *et al*. reported a lower Dslow value at 3 T ($0.99\pm0.16\times10^{-3}$ mm^2/s) than 1.5 T ($1.12\pm0.16\times10^{-3}$ mm^2/s, P=0.005), and higher PF value at 3 T (19.0±5.5%) than at 1.5 T (16.0±4.1%). A higher PF value at 3 T than at 1.5 T was also noted in Barbieri *et al.*'s paper (37). Therefore Dslow and PF are likely to be field strength dependent. Although the image artifacts, e.g., susceptibility induced artifacts, are less pronounced at 1.5 T than at 3 T; the relatively low SNR may compromise the precision of the calculated IVIM parameters.

Number of b values on IVIM parameters

IVIM parameters strongly depend upon the choice of the b value and the threshold used for computation. Including more b values and applying an optimized b value distribution reduces errors in the IVIM parameter estimates (16,34,49). ter Voert *et al.* (34) suggested the mean relative error of IVIM parameters depends on the number of b values and their distribution. In the calculated optimal IVIM protocols, the mean relative errors decreased by 40% or more when the number of b values included increased from 4 to 16. This effect is even more pronounced in inhomogeneous tumor compared with that in normal liver tissue. The recent ISMRM-Sponsored Workshop Consensus Statement on DW imaging outside the brain did not propose an IVIM data acquisition protocol (36). The optimal b value distribution has been suggested to be organ specific (41).

The overall impact of the number of values on IVIM parameters is shown with *Figure 4*. For Dslow and PF, an increase of total b value number or low b value number (<100 s/mm^2) leads to a decrease of CoV of individual studies. An increase of low b value (<100 s/mm^2) number and total b value number leads to a slight increase of Dslow value, a decrease of PF value, and a substantial increase of Dfast value. Together with the results of ter Voert *et al.* (34), it is probable that an accurately measured Dfast value is greater than what have been reported by most of the papers.

In ter Voert *et al.*'s study, including more b values and applying an optimized b value distribution significantly reduce errors in the IVIM parameter estimates, thereby increasing its accuracy. A useful b value distribution should have more b values in the 0 to 50 s/mm^2 range and fewer in the midrange of 450 to 800 s/mm^2 and up to 1,000 s/mm^2 (16). The largest gain in error reduction is in the range when moving from 4 to 11 b values. Therefore, ter Voert *et al.* suggest 11 b values an absolute minimum; usually 16 b values are needed (34). In ter Voert's study, the imaging time for IVIM was 5 to 6 minutes which is clinically acceptable. In these 5 to 6 minutes, they were able to acquire a 25 b value IVIM scan protocol. The distribution of the b values is also fundamental. The Dfast is more related to the low b values. This corresponds to the steep part in the measured signal versus b value graph. On *Figure 5* it can be seen that the curves are virtually parallel in the parts of 100–800 s/mm^2 (area almost exclusively influenced by Dslow); however they differ in the 0–100 s/mm^2 area which is the most sensitive part to differentiate the curves and most difficult to fit reliably, especially in the tissue with high perfusion factor. The problem with the published data is there were often few measurements in this part of the curve.

Respiratory triggering (RT) or free-breathing (FB) for liver data acquisition

Blurred images due to respiratory motion result in erroneous IVIM parameter estimation. Dyvorne *et al.* (15) found that RT sequence has higher image quality than FB sequences, the latter being much more prone to motion-related blurring. Additionally, left lobe may be more prone to cardiac motion artifacts which potentially can alter diffusion measurement (15). However, Barbieri *et al.* found that the use of RT did not have a significant effect on the measured parameter values (37).

Table 4 shows CoV of individual data of RT data acquisitions and FB data acquisitions, and no advantage of RT data is shown. It can be shown that only breath-hold (BH) can truly freeze the liver position, while RT is unavoidably associated with some extent of motion (*Figure 6*). It should be noted that respiratory and cardiac gating would roughly double the total IVIM acquisition time. Increasing the number of signal averages could also lead to blurring due to motion. Additionally, this does not change the errors due to Rician noise. With the limited data available, this review does not show that RT offers much advantage over FB, as the measured values were both scattered (*Figure 7*).

The larger relative error in tumor compared with that

Table 3 CoV of reported IVIM parameter acquired with 1.5 T* or 3 T**

CoV	Dslow ($\times 10^{-3}$ mm^2/s)	PF (%)	Dfast ($\times 10^{-3}$ mm^2/s)
CoV at 1.5 T	11.67%	34.35%	51.49%
CoV at 3 T	18.79%	39.46%	37.37%

*, 1.5 T data from references (10-12,15,20,22,23,42-47); **, 3.0 T data from references (9,19,21,24,40,41,48-55); CoV, coefficient of variation; IVIM, intravoxel incoherent motion.

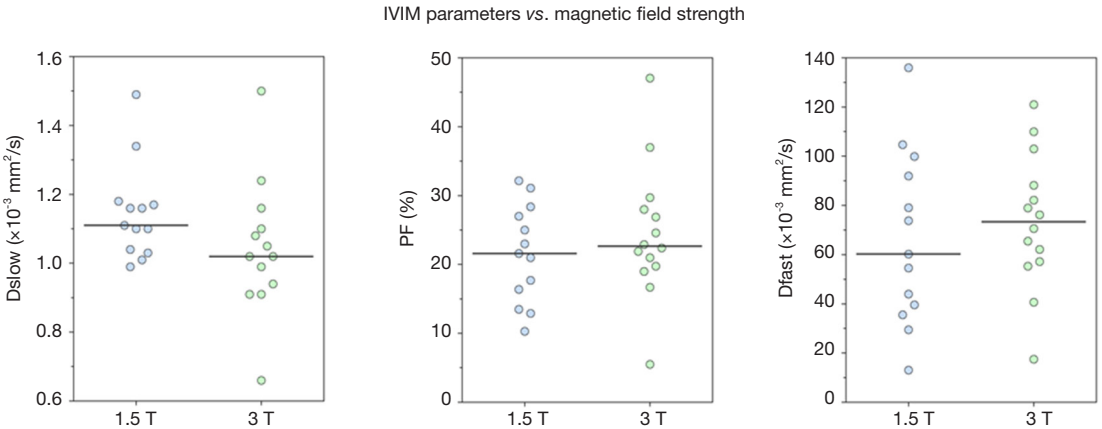

Figure 3 Dslow (D), perfusion fraction (PF), and Dfast (D*) values in healthy liver with data acquired with 1.5 T magnet or 3 T magnet. Solid line represents the median value of each group. PF, perfusion fraction.

in normal-appearing tissue could also be partially explained by motion and partial volume (34). Respiratory motion, cardiac motion and aortic pulsations cause the position of the tumor to move considerably during scanning. As a result, surrounding liver tissue could move in and out of the tumor ROIs. In addition, because tumor tissue is often less homogeneous than liver tissue, motion in a tumor ROI could have a larger effect on IVIM parameter estimation than motion in a normal liver ROI.

Only one study had breath-holding for a block of b values (44). This study shows that Dfast had a high value which agreed with the data of ter Voert *et al.* (34) using a high number of 25 b values. With fast data acquisition being continuously developed, breath-holding IVIM protocol should be further developed and validated.

Image post-processing methods for IVIM parameters

As IVIM processing requires complex modeling than does ADC measurement, the post-processing method should be sufficiently robust. Various fitting algorithms have been used to determine IVIM parameters, including asymptotic fitting (9-12,19-21,24,41,45,46,48,51,53), nonlinear least square (usually Levenberg-Marquardt) fitting (23,42,47,52,54,55), and Bayesian fitting (15,22,40,43,50). Current review cannot draw conclusion which one is better than others, nor can the mean values be compared (*Figure 8*).

Asymptotic fitting is the most commonly used method in the published IVIM studies. Asymptotic fitting is based on the assumption that the Dfast is much larger than Dslow and the impact of pseudo-diffusion on signal attenuation decreases with increasing b value, so Dslow can be calculated by fitting mono-exponential equation with large b value, where perfusion effects expected to be negligible. After Dslow been determined, PF and Dfast can be calculated by either stepwise or simultaneous fitting. For asymptotic method, it is essential to choose a threshold that separate diffusion and perfusion. According to Wurnig *et al.* (41), the optimal threshold is organ-specific, and, surprisingly liver. exhibited optimal thresholds of 20–40 s/mm^2 which is much lower than the thresholds used in the literature (150 or 200 s/mm^2). From a mathematical point of view this method has some limitations. Even in the first part of the curve (signal with b value under the

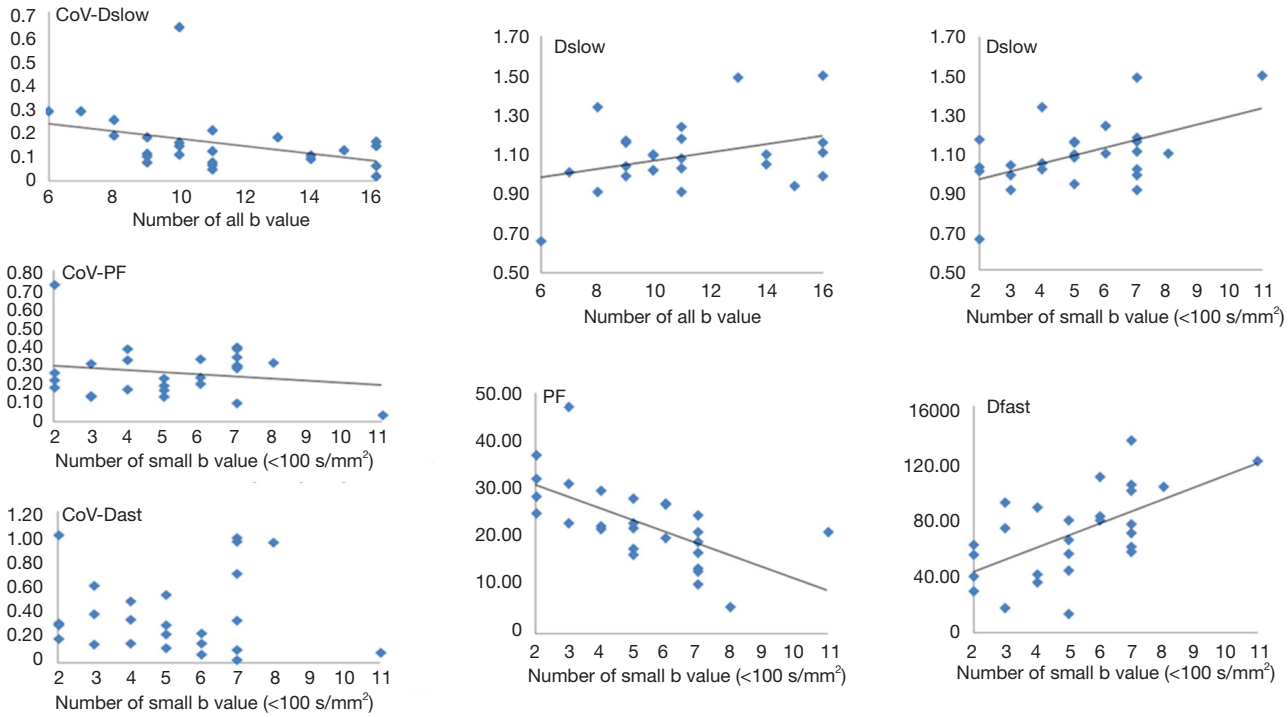

Figure 4 Variation of Dslow, CoV-Dslow, PF, Cov-PF, Dfast, and CoV-Dfast with the number of b value (all b value or small b value <100 s/mm^2). For Dslow and PF, an increase of the number of total b value or small b value (<100 s/mm^2) leads to a decrease of CoV of individual studies. An increase of the number of small b values (<100 s/mm^2) and total b values lead to a slight increase Dslow value. An increase of the number of small b values lead to a decrease of PF value, and a substantial increase of Dfast. CoV, coefficient of variation; PF, perfusion fraction.

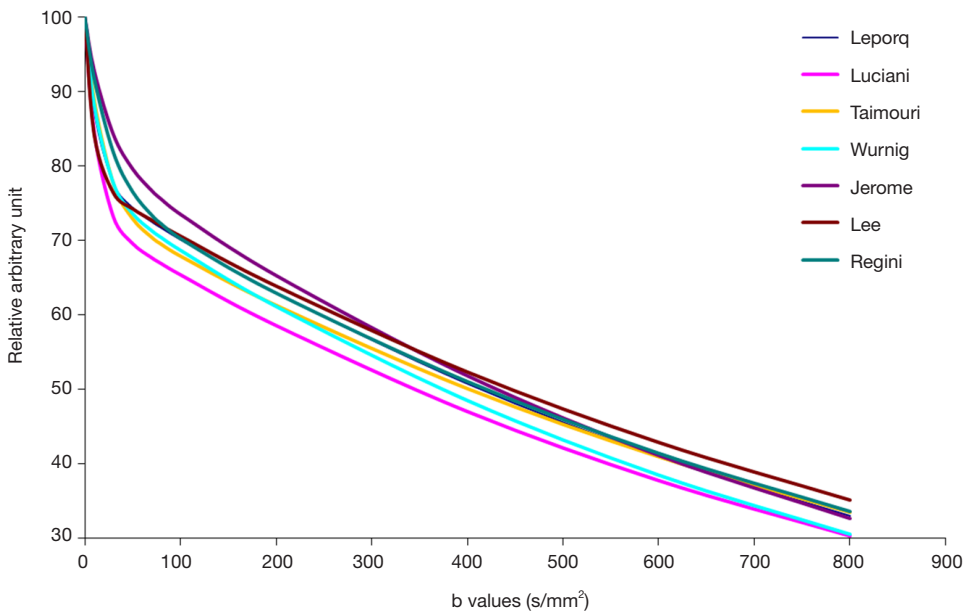

Figure 5 The reconstructed curves of diffusion weighted (DW) signals (Y-axis, relative arbitrary unit) with respect to the applied b values (X-axis, s/mm^2) based on the published values of normal liver parenchyma. Data from references (11,19,20,22-24,41).

Table 4 CoV of individual data of RT data acquisition* and FB data acquisition**

CoV	Dslow ($\times10^{-3}$ mm^2/s)	PF (%)	Dfast ($\times10^{-3}$ mm^2/s)
CoV of RT data (n=17)	17.06%	40.41%	51.04%
CoV of FB data (n=6)	8.72%	16.90%	24.00%

*, RT data acquisitions data from references (9-11,15,23,24,42,43,45,46,48,51,53-55); **, FB data acquisitions from references (19-21,40,41,47). CoV, coefficient of variation; RT, respiratory triggering; PF, perfusion fraction; FB, free-breathing.

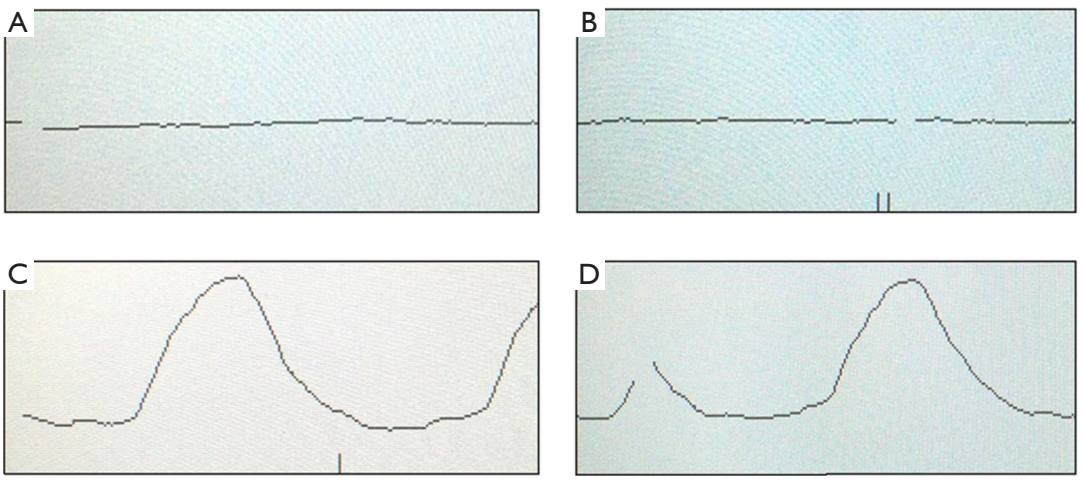

Figure 6 Screen shot of respiratory triggering (RT) window screen. (A,B) The subject was holding the breath, the diagram show a straight line; (C,D) the subject was free-breathing (FB). It can be expected that even RT cannot satisfactorily freeze the liver.

threshold) Dslow-related signal still accounts for a large fraction of the measured signal. However this information sometimes, depending on the fitting models, is not included for Dslow calculation. Furthermore, for reliable measurement, it is necessary to have high b values (around 800 s/mm^2) where SNR is low and the noise may be no longer in Gaussian distribution, in particular when there is an iron overload. This tends to underestimate Dslow and finally errors of Dslow calculation can be brought into the rest of calculation and degrade the other results.

Another widely used method is simultaneous non-linear least square fitting which estimates three parameters at the same time, usually based on Levenberg-Marquardt algorithm. Different from asymptotic fitting that optimizes the measurement of Dslow, it gives an identical weight to each variable. However, it has been reported that least-squares fitting has less stability compared to asymptotic fitting since it is sensitive to data outliers and image noise (38,48,53).

Bayesian-fitting approach has been recommended for IVIM parameter determination recently. Rather than calculating and minimizing an error residual, the Bayesian method yields estimates of the uncertainty of each parameter in the model and uses prior distributions on PF, Dfast, and Dslow to determine the joint posterior probability over all parameters, given a set of measured b value samples (56). It has been shown in previous IVIM studies that it is more stable against signal fluctuations than least-squares fitting approach, especially when SNR is low (17,38,56).

The choice of fitting algorithm should be based on the purpose and dataset of study. It has been proposed to average multiple data points per patient in order to improve the SNR and image quality (22,33). Another possible way to increase SNR is to scan with duplicated b values and rejecting data points that are affected by motion during post-processing. This way, the increased scan time could lead to an increase in SNR, depending on the number of data points that are not rejected. Instead of rejecting data points, perform motion correction is

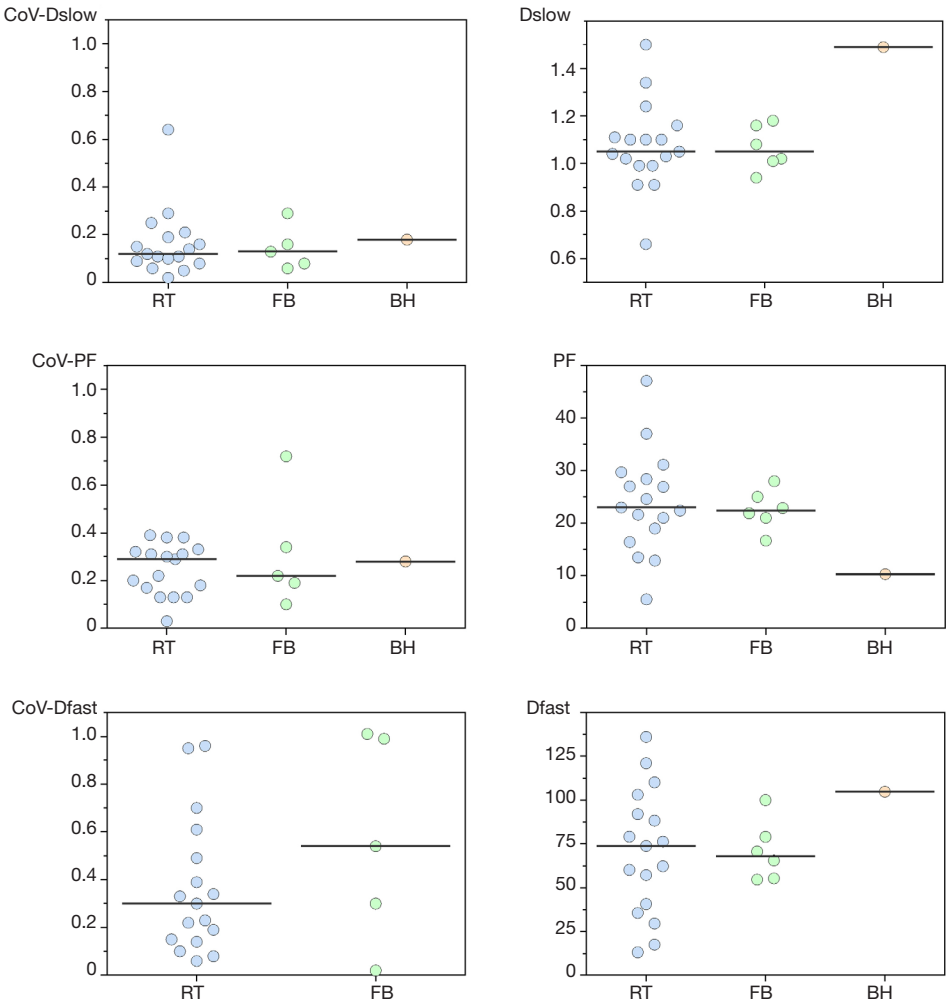

Figure 7 Values and coefficient of variation (CoV) of Dslow (D), perfusion fraction (PF), and Dfast (D*) in healthy liver parenchyma with data acquired by respiratory triggering (RT) (9-11,15,23,24,42,43,45,46,48-51,53-55), free-breathing (FB) (19-21,40,41,47), and breath-hold (BH) (44). Solid line represents the median value of each group.

another approach. As the high b value images have only a limited amount of signal and are therefore difficult to register, data can be collected with alternating low b value and high b value scans.

Other post-processing technique such as image de-noising and registration may also be helpful for IVIM quantification. These processing could potentially be more effective if it is applied on the images of the individual directions before averaging or directly on the raw data, which has not been attempted with IVIM study (35). However, it should be noted that the noise characteristics on MR magnitude images are much dependent on many factors of hardware, acquisition and reconstruction. Inappropriate de-noising technique simply applying on magnitude MR images may potentially alter the supposed bi-exponential decay in IVIM.

IVIM for liver fibrosis evaluation

Liver fibrosis is associated with a progressive increase in connective tissue. The increased proportion of collagen fibers impairs Brownian water motion within fibrotic livers. Accumulation of collagen deposits and activated stellate cells contribute to increased hepatic resistance to portal blood flow, development of portal hypertension, and reduced portal blood perfusion. The decrease of blood perfusion can arise from a number of concomitant alterations in the tissue microenvironment, including collagen deposition, fatty

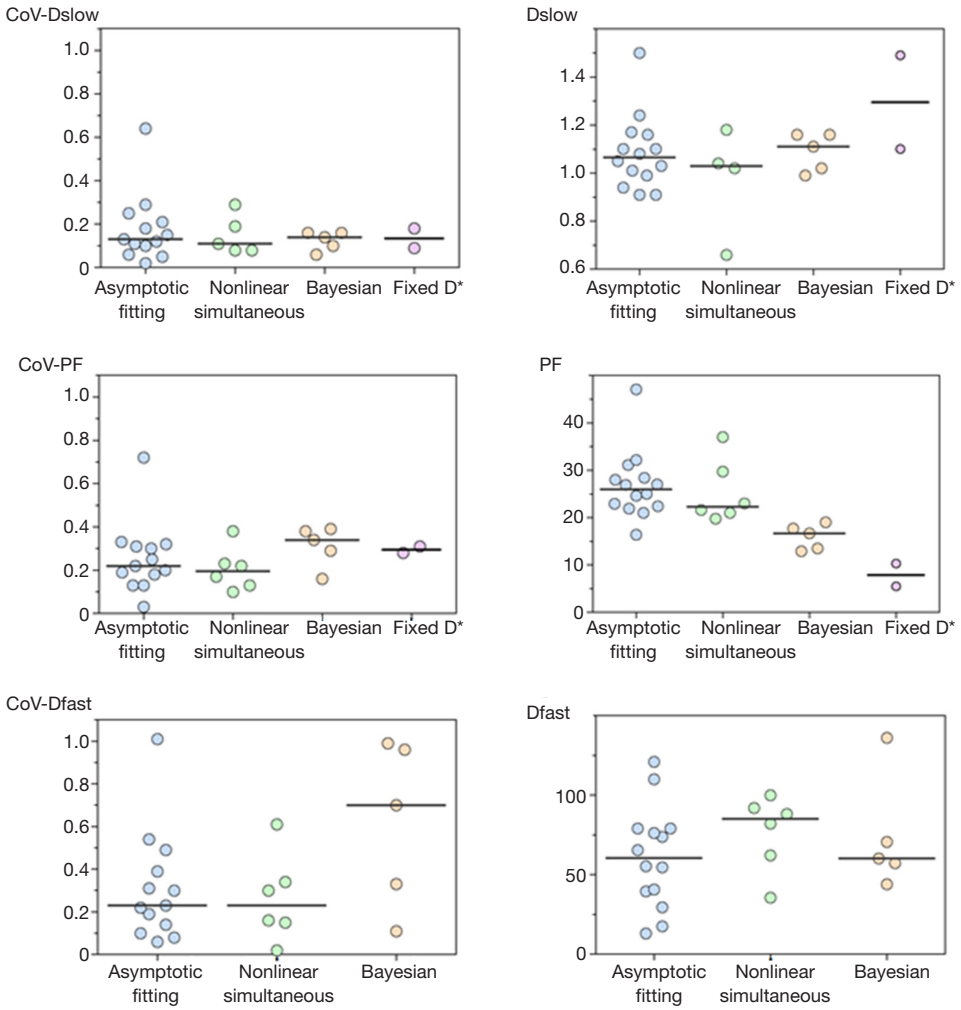

Figure 8 Values and coefficient of variation (CoV) of Dslow (D), perfusion fraction (PF), and Dfast (D*) in healthy liver parenchyma with data acquired with asymptotic fitting (n=14), nonlinear simultaneous fitting (n=6), Bayesian fitting (n=5), and fixed Dfast fitting (n=2). Solid line represents the median value of each group.

infiltration, hepatitis, cell necrosis/apoptosis, inflammatory cell infiltration, and fibroblast proliferation with different degrees. The relative short T2 and T2* of liver tissue, coupled with susceptibility effect, motion, the presence of fatty tissue and highly variable iron content, makes it challenging to apply IVIM for liver.

With IVIM technique, Luciani *et al.* reported that Dfast was significantly reduced in the liver fibrosis compared with those in the healthy liver group, but there was no significant difference between Dslow and PF measurements in the healthy liver (n=25) and the liver fibrosis (n=12) groups (11). Guiu *et al.* (9) reported that Dslow and Dfast were significantly lower in steatotic compared with nonsteatotic livers; however, PF was significantly higher in steatotic compared with nonsteatotic livers. In another study, Patel *et al.* (12) reported that the value of Dslow, PF and Dfast in liver cirrhosis were lower than non-cirrhosis liver; however, no further grading was performed within their liver cirrhosis subjects as only three patients had histopathology data. In a rat model of diethylnitrosamine-induced liver fibrosis, Zhang *et al.* (57) reported that PF values decreased significantly with the increasing fibrosis level; but Dslow was poorly correlated with fibrosis level. In a carbon tetrachloride induced rat liver fibrosis model, Chow *et al.* (58) reported that as liver fibrosis progressed, Dslow and Dfast decreased, however there was no change in PF. Joo *et al.* (59) reported that PF was significantly lower in rabbits with nonalcoholic fatty liver disease than in those

with a normal liver, and it decreased further as severity of nonalcoholic fatty liver disease increased; however, Dslow and Dfast did not differ significantly between the nonalcoholic fatty liver disease severity groups.

In a relatively large cohort study including 17 healthy volunteers and 34 patients with histopathologically confirmed liver fibrosis patients (stage 1=14, stage 2=8, stage 3 & 4=12, METAVIR grading), and with a 1.5 T magnet and 10 b values, Lu *et al.* (10) reported Dslow, PF, and Dfast in healthy volunteer livers and patient livers were 1.096±0.155 *vs.* 0.917±0.152 ($\times 10^{-3}$ mm^2/s, P=0.0015), 0.164±0.021 *vs.* 0.123±0.029 (P=0.0001), and 13.085±2.943 *vs.* 9.423±1.737 ($\times 10^{-3}$ mm^2/s, P=0.0001) respectively, all significantly lower in fibrotic livers. As the fibrosis severity progressed, Dslow, PF, and Dfast values decreased, with a significant trend for PF and Dfast (*Figure 9*). However, due to the large overlap of Dslow, PF, and Dfast for different fibrosis stages, they cannot be used to diagnose liver fibrosis, nor could they reliably differentiate fibrosis of different stages (*Figure 10*).

IVIM technique for liver tumor detection and differentiation

A number of studies reported IVIM technique for liver tumor diagnostic evaluation. Liver nodules include hepatocellular carcinoma (HCC), hemangioma, focal nodular hyperplasias (FNH), liver metastasis (MET) or malignant nodules (MAL, pathology not specified) (*Figures 11,12*). *Figures 11,12* showed overlap of value of IVIM parameters for liver parenchyma and various pathologies. It can be seen that IVIM technique has yet to show the capability to detect or diagnose liver tumors.

IVIM techniques for liver tumor therapeutic effect monitoring

Pilot studies have been published and demonstrated the feasibility of using IVIM to monitor and follow-up therapies, mostly on animal models. However, the relatively low reproducibility of PF and Dfast hinders their use as quantitative biomarkers (15). The PF of regions at a large tumor's core is generally lower than that of the liver, which means that the signal allowing the measurement of Dfast is even lower, which will further decrease the reliability of the measurement.

Vascular disrupting agent (VDA) acts on existing tumor blood vessels and induce acute collapse of the immature tumor vasculature. Because these treatments may be effective without initially reducing tumor size, quantitative imaging of tumor perfusion is being investigated as an early response and predictive biomarker. Contrast-enhanced ultrasonography, computed tomography, and MRI have been used to quantify tumor perfusion before and after antivascular treatments, and decrease in such imaging parameters has been demonstrated in responders (60). In an implanted rabbit VX2 liver tumor model, in 2014 Joo *et al.* (61) demonstrated PF and Dslow significantly decreased 4 hours after administration of a VDA (CKD-516, Chong Kun Dang Pharmaceutical Corp., S. Korea). A larger decrease in the perfusion-sensitive IVIM parameters was correlated with smaller tumor size increase 7 days after treatment. In their study IVIM protocol was performed at 3 T and using 12 increasing diffusion weightings (b values, 0–800 s/mm^2), with at least eight of these in the low-b value perfusion-sensitive range. Further study from the same group demonstrated that Dfast and PF had significant positive correlations with DCE parameters K(trans) and initial area under the gadolinium concentration-time curve (iAUC until 60 seconds) (62). Yang *et al.* (63) reported the usefulness of PF for the assessment of the therapeutic efficacy of Sorafenib (Nexavar®, Bayer and Onyx Pharmaceuticals) in a mice orthotopic HCC model, before and after 6 weeks each treatment was performed at 1.5 T with b0=0 s/mm^2, b1=50 s/mm^2, b2=800s/mm^2.

Pieper *et al.* (64) described a human subject study using IVIM analysis for evaluation of therapy-induced tumor changes and response of breast cancer liver metastases undergoing radioembolization. The authors suggested that PF can deliver additional information over tumor size changes and long-term RECIST response after radioembolization of breast cancer liver metastases.

Conclusions

A reasonable range of Dslow and PF for a healthy liver can be estimated. For future studies if Dslow and PF of liver fall out of reasonable range, causes should be investigated. Imperfection in data acquisition or processing method may lead to reduced sensitivity in detecting tissue changes (65,66). Systematic bias may also be introduced during imaging due to difference of hardware being used. The medium values or mean value of IVIM parameters presented in this review do not necessarily, or even unlikely, represent the true value or physiological value. However, if a value is consistently measured, and allow differentiating pathologies,

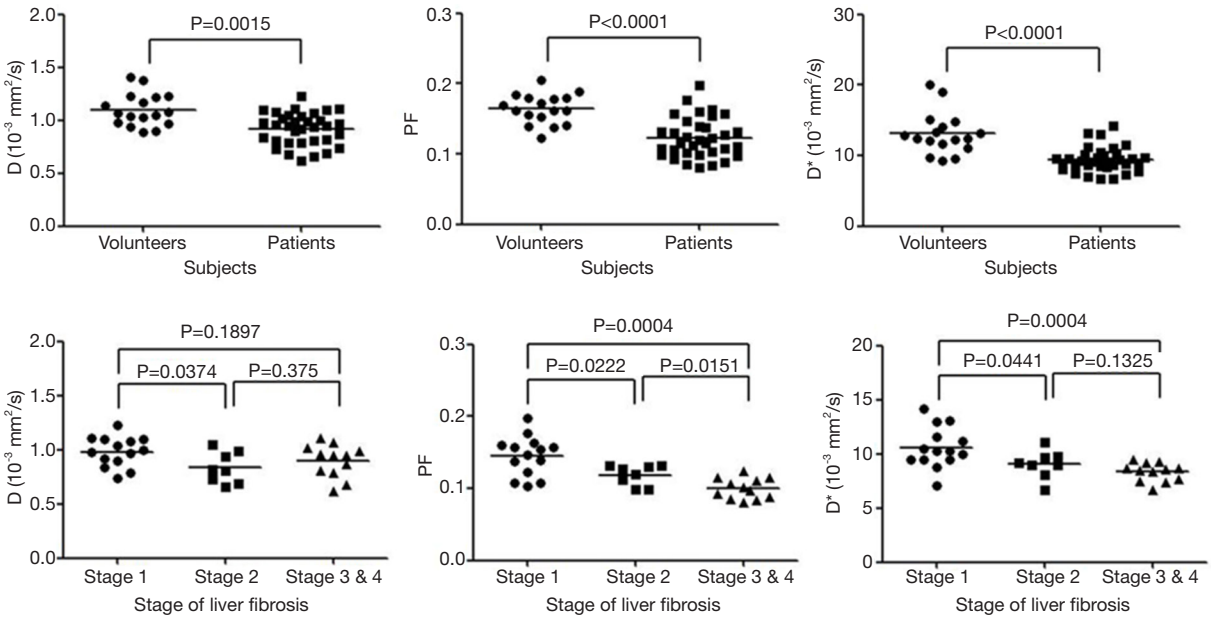

Figure 9 Dslow (D), perfusion fraction (PF), and Dfast (D*) values in healthy livers (n=17) and fibrotic livers (n=34). Dslow, PF, and Dfast are significantly lower in fibrotic livers than in healthy livers. As the fibrosis severity progressed, Dslow, PF, and Dfast values decreased, with a trend significant for PF and Dfast. However, large overlaps among the values exist [original data from (10)].

then it can be regarded as reliable "apparent" value. This review shows the reported IVIM parameter Dfast is rather heterogeneous. Except for increasing the number of b value can decrease the CoV of Dslow, with the published data we did not see other factors such as higher magnetic field strength or respiratory gating (*vs.* FB) substantially improve measurement precision of PF or Dfast. Such heterogeneities lead to the doubt that the clinical applicability of the IVIM parameters over the accepted ADC which may also use multiple b values (8). This review shows the currently reported IVIM technique may still not be able to reliably detect early fibrosis or differentiate fibrosis grades, or contribute to tumor diagnosis in a meaningful way.

Though limited studies showed IVIM technique may be able to monitor liver tumor treatment response, its cost-effectiveness and inter-sites consistency compared with other simpler approaches remains unknown. In fact, Klauss *et al.* (67) suggested that ADC performed equally to IVIM-derived parameters, a straightforward ADC measurement may be sufficient for DW imaging, which is possible if the acquisition protocol is fixed and that the different variables are managed in a coordinated way.

Moreover, improving the reliability of the measures require a better understanding of the physiology of different micro-perfusion regions. It remains uncertain whether the speed of water molecule is distributed according to statistical normal distribution pattern in both the intravascular and the interstitial spaces; as this could lead to the increased complexity of the model because the perfusion circulation at these two regions are quite different. To have a deeper understanding of this point as well as being able to demonstrate the difference or sameness would provide another aspect of the usefulness of diffusion imaging.

For IVIM technique to be reliably applied in abdominal organ, more technical innovations are warranted. Since there are three variables in Eq. [1], accurate fitting of the IVIM parameters demands robust and reliable relations between signals and b values. Methods to freeze the breathing motion and increase SNR per b value acquisition may be explored first of all, as they induce major sources of measurement imprecision. Improving the methods of calculation is another major topic where progresses are possible, such as mathematical modelling, the integration of de-noising with different statistical models, and management of artifacts. Additionally, the relationship between Dslow, as derived from the biexponential model between signals and b values (Eq. [1]), and ADC value which is derived by taking the assumption of mono-exponential relationship between signals and b values, requires in-depth exploration.

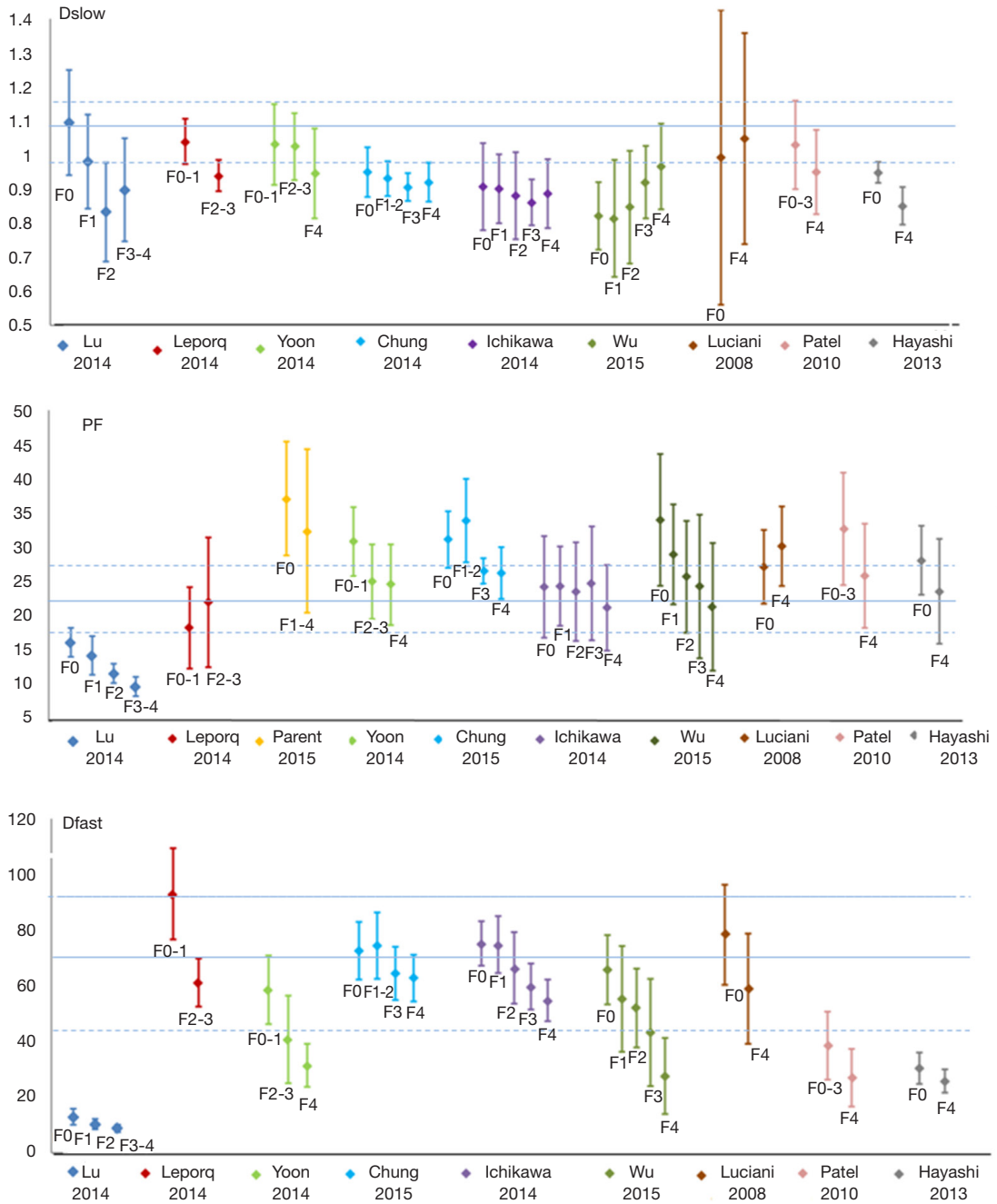

Figure 10 Mean and standard deviation (SD) of Dslow (D, 10^{-3} mm^2/s), perfusion fraction (PF, %), and Dfast (D*, 10^{-3} mm^2/s) values in healthy liver and fibrotic livers (n=10). As the fibrosis severity progressed, Dslow, PF, and Dfast values decreased. However, large overlaps among the values exist. Blue solid line represents median values of reported healthy liver intravoxel incoherent motion (IVIM) parameters. Regions between blue dash lines represent mid 50% data (middle two quartiles) distribution of reported healthy liver value.

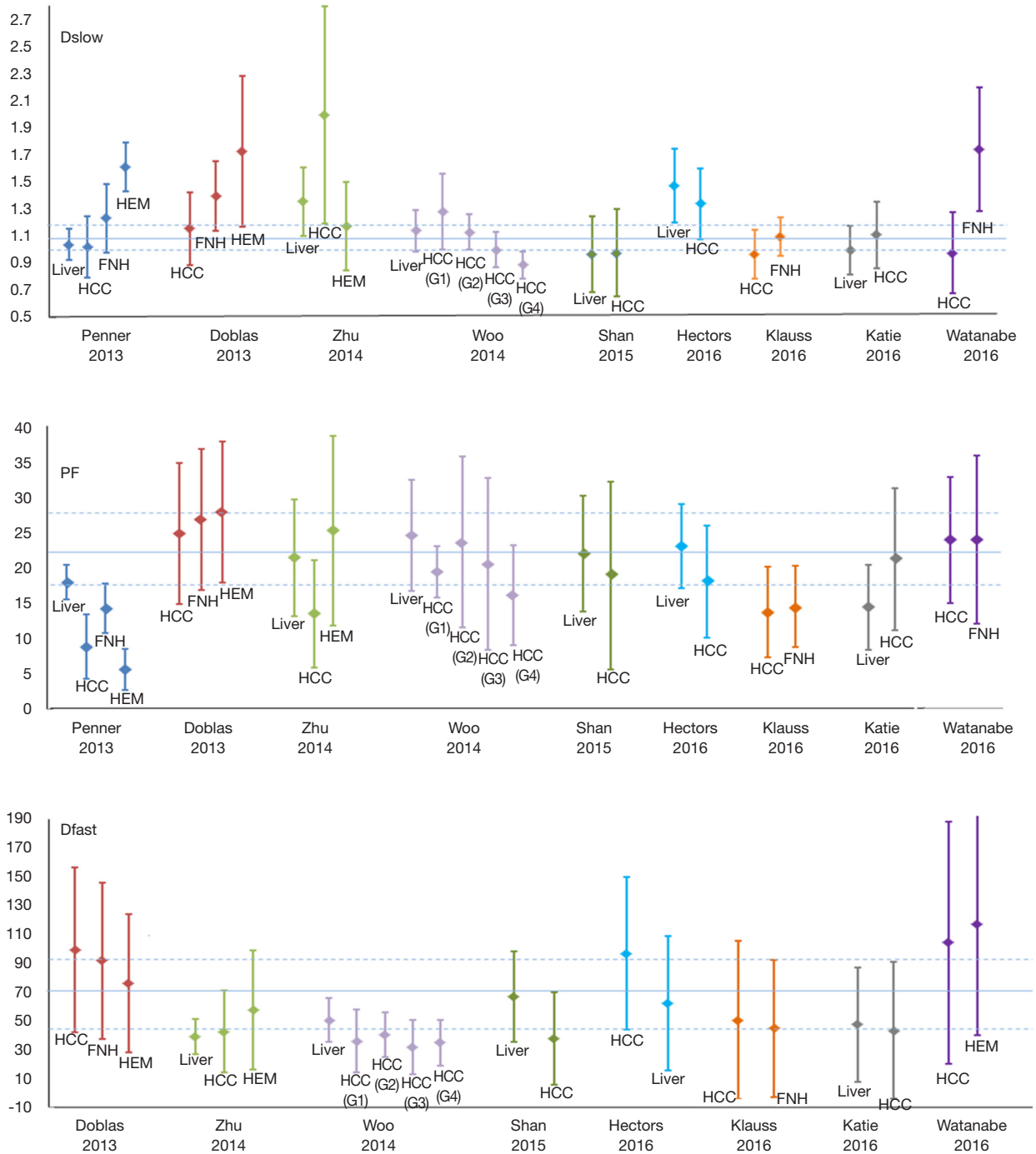

Figure 11 Mean and standard deviation (SD) of Dslow (D, 10^{-3} mm^2/s), perfusion fraction (PF, %), and Dfast (D*, 10^{-3} mm^2/s) values in healthy liver parenchyma and liver tumors, including hepatocellular carcinomas (HCC), focal nodular hyperplasias (FNH), haemangioma (HEM). Blue solid line represents median values of reported healthy liver intravoxel incoherent motion (IVIM) parameters. Regions between blue dash lines represent mid 50% data (middle two quartiles) distribution of reported healthy liver value.

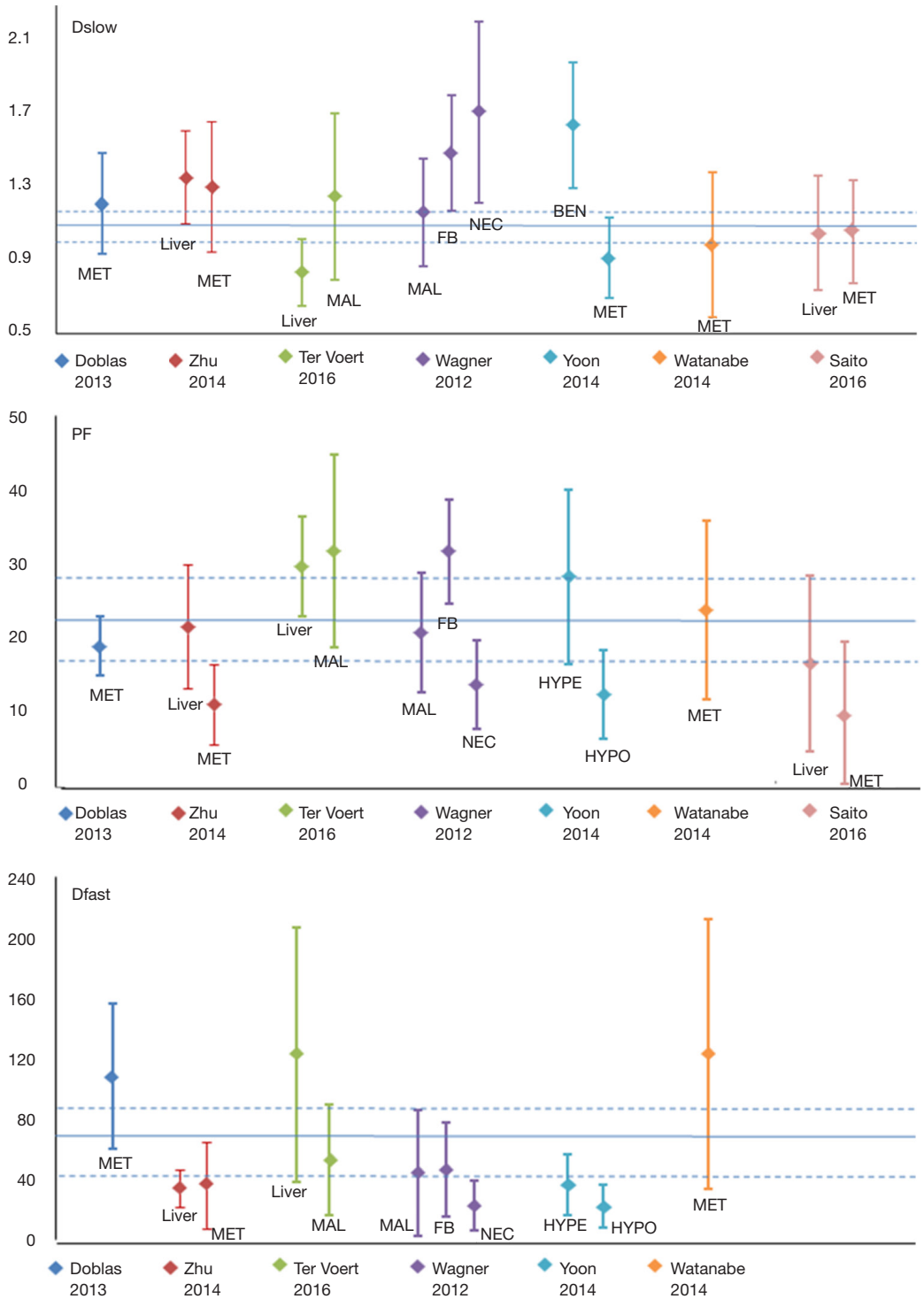

Figure 12 Mean and standard deviation (SD) of Dslow (D, 10^{-3} mm^2/s), perfusion fraction (PF, %), and Dfast (D*, 10^{-3} mm^2/s) values in healthy liver parenchyma (liver) and metastasis (MET) and malignant nodules (MAL, pathology not specified), fibrous region (FB), necrotic region (NEC). Blue solid line represents median values of reported healthy liver intravoxel incoherent motion (IVIM) parameters. Regions between blue dash lines represent mid 50% data distribution (middle two quartiles) of reported healthy liver value. HYPE, hypervascular; HYPO, hypovascular.

Acknowledgements

None.

Footnote

Conflicts of Interest: The authors have no conflicts of interest to declare.

References

1. Le Bihan D, Breton E, Lallemand D, Aubin ML, Vignaud J, Laval-Jeantet M. Separation of diffusion and perfusion in intravoxel incoherent motion MR imaging. Radiology 1988;168:497-505.
2. Koh DM, Collins DJ. Diffusion-weighted MRI in the body: applications and challenges in oncology. AJR Am J Roentgenol 2007;188:1622-35.
3. Le Bihan D, Breton E, Lallemand D, Grenier P, Cabanis E, Laval-Jeantet M. MR imaging of intravoxel incoherent motions: application to diffusion and perfusion in neurologic disorders. Radiology 1986;161:401-7.
4. Le Bihan D, Turner R. The capillary network: a link between IVIM and classical perfusion. Magn Reson Med 1992;27:171-8.
5. Le Bihan D, Turner R, Moonen CT, Pekar J. Imaging of diffusion and microcirculation with gradient sensitization: design, strategy, and significance. J Magn Reson Imaging 1991;1:7-28.
6. Murphy P, Hooker J, Ang B, Wolfson T, Gamst A, Bydder M, Middleton M, Peterson M, Behling C, Loomba R, Sirlin C. Associations between histologic features of nonalcoholic fatty liver disease (NAFLD) and quantitative diffusion-weighted MRI measurements in adults. J Magn Reson Imaging 2015;41:1629-38.
7. Yamada I, Aung W, Himeno Y, Nakagawa T, Shibuya H. Diffusion coefficients in abdominal organs and hepatic lesions: evaluation with intravoxel incoherent motion echo-planar MR imaging. Radiology 1999;210:617-23.
8. Guiu B, Cercueil JP. Liver diffusion-weighted MR imaging: the tower of Babel? Eur Radiol 2011;21:463-7.
9. Guiu B, Petit JM, Capitan V, Aho S, Masson D, Lefevre PH, Favelier S, Loffroy R, Vergès B, Hillon P, Krausé D, Cercueil JP. Intravoxel incoherent motion diffusion-weighted imaging in nonalcoholic fatty liver disease: a 3.0-T MR study. Radiology 2012;265:96-103.
10. Lu PX, Huang H, Yuan J, Zhao F, Chen ZY, Zhang Q, Ahuja AT, Zhou BP, Wáng YX. Decreases in molecular diffusion, perfusion fraction and perfusion-related diffusion in fibrotic livers: a prospective clinical intravoxel incoherent motion MR imaging study. PLoS One 2014;9:e113846.
11. Luciani A, Vignaud A, Cavet M, Nhieu JT, Mallat A, Ruel L, Laurent A, Deux JF, Brugieres P, Rahmouni A. Liver cirrhosis: intravoxel incoherent motion MR imaging--pilot study. Radiology 2008;249:891-9.
12. Patel J, Sigmund EE, Rusinek H, Oei M, Babb JS, Taouli B. Diagnosis of cirrhosis with intravoxel incoherent motion diffusion MRI and dynamic contrast-enhanced MRI alone and in combination: preliminary experience. J Magn Reson Imaging 2010;31:589-600.
13. Grech-Sollars M, Hales PW, Miyazaki K, Raschke F, Rodriguez D, Wilson M, Gill SK, Banks T, Saunders DE, Clayden JD, Gwilliam MN, Barrick TR, Morgan PS, Davies NP, Rossiter J, Auer DP, Grundy R, Leach MO, Howe FA, Peet AC, Clark CA. Multi-centre reproducibility of diffusion MRI parameters for clinical sequences in the brain. NMR Biomed 2015;28:468-85.
14. Wang YX. Medical imaging in pharmaceutical clinical trials: what radiologists should know. Clin Radiol 2005;60:1051-7.
15. Dyvorne HA, Galea N, Nevers T, Fiel MI, Carpenter D, Wong E, Orton M, de Oliveira A, Feiweier T, Vachon ML, Babb JS, Taouli B. Diffusion-weighted imaging of the liver with multiple b values: effect of diffusion gradient polarity and breathing acquisition on image quality and intravoxel incoherent motion parameters--a pilot study. Radiology 2013;266:920-9.
16. Lemke A, Stieltjes B, Schad LR, Laun FB. Toward an optimal distribution of b values for intravoxel incoherent motion imaging. Magn Reson Imaging 2011;29:766-76.
17. Andreou A, Koh DM, Collins DJ, Blackledge M, Wallace T, Leach MO, Orton MR. Measurement reproducibility of perfusion fraction and pseudodiffusion coefficient derived by intravoxel incoherent motion diffusion-weighted MR imaging in normal liver and metastases. Eur Radiol 2013;23:428-34.
18. Chen C, Wang B, Shi D, Fu F, Zhang J, Wen Z, Zhu S, Xu J, Lin Q, Li J, Dou S. Initial study of biexponential model of intravoxel incoherent motion magnetic resonance imaging in evaluation of the liver fibrosis. Chin Med J (Engl) 2014;127:3082-7.
19. Leporq B, Saint-Jalmes H, Rabrait C, Pilleul F, Guillaud O, Dumortier J, Scoazec JY, Beuf O. Optimization of intra-voxel incoherent motion imaging at 3.0 Tesla for fast liver examination. J Magn Reson Imaging 2015;41:1209-17.

20. Taimouri V, Afacan O, Perez-Rossello JM, Callahan MJ, Mulkern RV, Warfield SK, Freiman M. Spatially constrained incoherent motion method improves diffusion-weighted MRI signal decay analysis in the liver and spleen. Med Phys 2015;42:1895-903.
21. Wurnig MC, Kenkel D, Filli L, Boss A. A Standardized Parameter-Free Algorithm for Combined Intravoxel Incoherent Motion and Diffusion Kurtosis Analysis of Diffusion Imaging Data. Invest Radiol 2016;51:203-10.
22. Jerome NP, Orton MR, d'Arcy JA, Collins DJ, Koh DM, Leach MO. Comparison of free-breathing with navigator-controlled acquisition regimes in abdominal diffusion-weighted magnetic resonance images: Effect on ADC and IVIM statistics. J Magn Reson Imaging 2014;39:235-40.
23. Lee Y, Lee SS, Kim N, Kim E, Kim YJ, Yun SC, Kühn B, Kim IS, Park SH, Kim SY, Lee MG. Intravoxel incoherent motion diffusion-weighted MR imaging of the liver: effect of triggering methods on regional variability and measurement repeatability of quantitative parameters. Radiology 2015;274:405-15.
24. Regini F, Colagrande S, Mazzoni LN, Busoni S, Matteuzzi B, Santini P, Wyttenbach R. Assessment of Liver Perfusion by IntraVoxel Incoherent Motion (IVIM) Magnetic Resonance-Diffusion-Weighted Imaging: Correlation With Phase-Contrast Portal Venous Flow Measurements. J Comput Assist Tomogr 2015;39:365-72.
25. Carter JH, Welch CS, Barron RE. Changes in the hepatic blood vessels in cirrhosis of the liver. Surg Gynecol Obstet 1961;113:133-7.
26. Bearn AG, Billing B, Sherlock S.The effect of adrenaline and noradrenaline on hepatic blood flow and splanchnic carbohydrate metabolism in man. J Physiol 1951;115:430-41.
27. Loisance DY, Lenriot JP. Critical review of methods of measurement of hepatic blood flow in animal experimentation and human clinical practice. Coeur Med Interne 1972;11:547-57.
28. Chow PK, Yu WK, Soo KC, Chan ST. The measurement of liver blood flow: a review of experimental and clinical methods. J Surg Res 2003;112:1-11.
29. Greenway CV, Stark RD. Hepatic vascular bed. Physiol Rev 1971;51:23-65.
30. Strandell T, Erwald R, Kulling KG, Lundbergh P, Marions O, Wiechel KL. Measurement of dual hepatic blood flow in awake patients. J Appl Physiol 1973;35:755-61.
31. Magalotti D, Volta U, Bonfiglioli A, Ramilli S, Berzigotti A, Zoli M. Splanchnic haemodynamics in patients with coeliac disease: effects of a gluten-free diet. Dig Liver Dis 2003;35:262-8.
32. Glick Z, Wickler SJ, Stern JS, Horwitz BA. Regional blood flow in rats after a single low-protein, high-carbohydrate test meal. Am J Physiol 1984;247:R160-6.
33. Lemke A, Laun FB, Simon D, Stieltjes B, Schad LR. An in vivo verification of the intravoxel incoherent motion effect in diffusion-weighted imaging of the abdomen. Magn Reson Med 2010;64:1580-5.
34. ter Voert EE, Delso G, Porto M, Huellner M, Veit-Haibach P. Intravoxel Incoherent Motion Protocol Evaluation and Data Quality in Normal and Malignant Liver Tissue and Comparison to the Literature. Invest Radiol 2016;51:90-9.
35. Hectors SJ, Wagner M, Besa C, Bane O, Dyvorne HA, Fiel MI, Zhu H, Donovan M, Taouli B. Intravoxel incoherent motion diffusion-weighted imaging of hepatocellular carcinoma: Is there a correlation with flow and perfusion metrics obtained with dynamic contrast-enhanced MRI? J Magn Reson Imaging 2016;44:856-64.
36. Taouli B, Beer AJ, Chenevert T, Collins D, Lehman C, Matos C, Padhani AR, Rosenkrantz AB, Shukla-Dave A, Sigmund E, Tanenbaum L, Thoeny H, Thomassin-Naggara I, Barbieri S, Corcuera-Solano I, Orton M, Partridge SC, Koh DM. Diffusion-weighted imaging outside the brain: Consensus statement from an ISMRM-sponsored workshop. J Magn Reson Imaging 2016;44:521-40.
37. Barbieri S, Donati OF, Froehlich JM, Thoeny HC. Comparison of Intravoxel Incoherent Motion Parameters across MR Imagers and Field Strengths: Evaluation in Upper Abdominal Organs. Radiology 2016;279:784-94.
38. Barbieri S, Donati OF, Froehlich JM, Thoeny HC. Impact of the calculation algorithm on biexponential fitting of diffusion-weighted MRI in upper abdominal organs. Magn Reson Med 2016;75:2175-84.
39. Pekar J, Moonen CT, van Zijl PC. On the precision of diffusion/perfusion imaging by gradient sensitization. Magn Reson Med 1992;23:122-9.
40. Kakite S, Dyvorne H, Besa C, Cooper N, Facciuto M, Donnerhack C, Taouli B. Hepatocellular carcinoma: short-term reproducibility of apparent diffusion coefficient and intravoxel incoherent motion parameters at 3.0T. J Magn Reson Imaging 2015;41:149-56.
41. Wurnig MC, Donati OF, Ulbrich E, Filli L, Kenkel D, Thoeny HC, Boss A. Systematic analysis of the intravoxel incoherent motion threshold separating perfusion and diffusion effects: Proposal of a standardized algorithm. Magn Reson Med 2015;74:1414-22.

42. Zhu L, Cheng Q, Luo W, Bao L, Guo G. A comparative study of apparent diffusion coefficient and intravoxel incoherent motion-derived parameters for the characterization of common solid hepatic tumors. Acta Radiol 2015;56:1411-8.
43. Dyvorne H, Jajamovich G, Kakite S, Kuehn B, Taouli B. Intravoxel incoherent motion diffusion imaging of the liver: optimal b-value subsampling and impact on parameter precision and reproducibility. Eur J Radiol 2014;83:2109-13.
44. Delattre BM, Viallon M, Wei H, Zhu YM, Feiweier T, Pai VM, Wen H, Croisille P. In vivo cardiac diffusion-weighted magnetic resonance imaging: quantification of normal perfusion and diffusion coefficients with intravoxel incoherent motion imaging. Invest Radiol 2012;47:662-70.
45. Hayashi T, Miyati T, Takahashi J, Fukuzawa K, Sakai H, Tano M, Saitoh S. Diffusion analysis with triexponential function in liver cirrhosis. J Magn Reson Imaging 2013;38:148-53.
46. Chung SR, Lee SS, Kim N, Yu ES, Kim E, Kühn B, Kim IS. Intravoxel incoherent motion MRI for liver fibrosis assessment: a pilot study. Acta Radiol 2015;56:1428-36.
47. Leitão HS, Doblas S, d'Assignies G, Garteiser P, Daire JL, Paradis V, Geraldes CF, Vilgrain V, Van Beers BE. Fat deposition decreases diffusion parameters at MRI: a study in phantoms and patients with liver steatosis. Eur Radiol 2013;23:461-7.
48. Cercueil JP, Petit JM, Nougaret S, Soyer P, Fohlen A, Pierredon-Foulongne MA, Schembri V, Delhom E, Schmidt S, Denys A, Aho S, Guiu B. Intravoxel incoherent motion diffusion-weighted imaging in the liver: comparison of mono-, bi- and tri-exponential modelling at 3.0-T. Eur Radiol 2015;25:1541-50.
49. Gurney-Champion OJ, Froeling M, Klaassen R, Runge JH, Bel A, van Laarhoven HW, Stoker J, Nederveen AJ. Minimizing the Acquisition Time for Intravoxel Incoherent Motion Magnetic Resonance Imaging Acquisitions in the Liver and Pancreas. Invest Radiol 2016;51:211-20.
50. Cui Y, Dyvorne H, Besa C, Cooper N, Taouli B. IVIM Diffusion-weighted Imaging of the Liver at 3.0T: Comparison with 1.5T. Eur J Radiol Open 2015;2:123-8.
51. Ichikawa S, Motosugi U, Morisaka H, Sano K, Ichikawa T, Enomoto N, Matsuda M, Fujii H, Onishi H. MRI-based staging of hepatic fibrosis: Comparison of intravoxel incoherent motion diffusion-weighted imaging with magnetic resonance elastography. J Magn Reson Imaging 2015;42:204-10.
52. Gambarota G, Hitti E, Leporq B, Saint-Jalmes H, Beuf O. Eliminating the blood-flow confounding effect in intravoxel incoherent motion (IVIM) using the non-negative least square analysis in liver. Magn Reson Med 2017;77:310-7.
53. Filli L, Wurnig MC, Luechinger R, Eberhardt C, Guggenberger R, Boss A. Whole-body intravoxel incoherent motion imaging. Eur Radiol 2015;25:2049-58.
54. Zhang J, Guo Y, Tan X, Zheng Z, He M, Xu J, Mei Y, Zhang J, Zhao X, Wang C, Feng Y, Chan Q, Wu Y, Xu Y. MRI-based estimation of liver function by intravoxel incoherent motion diffusion-weighted imaging. Magn Reson Imaging 2016;34:1220-5.
55. França M, Martí-Bonmatí L, Alberich-Bayarri Á, Oliveira P, Guimaraes S, Oliveira J, Amorim J, Gonzalez JS, Vizcaíno JR, Miranda HP. Evaluation of fibrosis and inflammation in diffuse liver diseases using intravoxel incoherent motion diffusion-weighted MR imaging. Abdom Radiol (NY) 2016 . [Epub ahead of print]. doi: 10.1007/s00261-016-0899-0
56. Neil JJ, Bretthorst GL. On the use of Bayesian probability theory for analysis of exponential decay data: an example taken from intravoxel incoherent motion experiments. Magn Reson Med 1993;29:642-7.
57. Zhang Y, Jin N, Deng J, Guo Y, White SB, Yang GY, Omary RA, Larson AC. Intra-voxel incoherent motion MRI in rodent model of diethylnitrosamine-induced liver fibrosis. Magn Reson Imaging 2013;31:1017-21.
58. Chow AM, Gao DS, Fan SJ, Qiao Z, Lee FY, Yang J, Man K, Wu EX. Liver fibrosis: an intravoxel incoherent motion (IVIM) study. J Magn Reson Imaging 2012;36:159-67.
59. Joo I, Lee JM, Yoon JH, Jang JJ, Han JK, Choi BI. Nonalcoholic fatty liver disease: intravoxel incoherent motion diffusion-weighted MR imaging-an experimental study in a rabbit model. Radiology 2014;270:131-40.
60. Wang YX, Deng M. Medical imaging in new drug clinical development. J Thorac Dis 2010;2:245-52.
61. Joo I, Lee JM, Han JK, Choi BI. Intravoxel incoherent motion diffusion-weighted MR imaging for monitoring the therapeutic efficacy of the vascular disrupting agent CKD-516 in rabbit VX2 liver tumors. Radiology 2014;272:417-26.
62. Joo I, Lee JM, Grimm R, Han JK, Choi BI. Monitoring Vascular Disrupting Therapy in a Rabbit Liver Tumor Model: Relationship between Tumor Perfusion Parameters at IVIM Diffusion-weighted MR Imaging and Those at Dynamic Contrast-enhanced MR Imaging. Radiology 2016;278:104-13.

63. Yang SH, Lin J, Lu F, Han ZH, Fu CX, Lv P, Liu H, Gao DM. Evaluation of antiangiogenic and antiproliferative effects of sorafenib by sequential histology and intravoxel incoherent motion diffusion-weighted imaging in an orthotopic hepatocellular carcinoma xenograft model. J Magn Reson Imaging 2017;45:270-80.
64. Pieper CC, Sprinkart AM, Meyer C, König R, Schild HH, Kukuk GM, Mürtz P. Evaluation of a Simplified Intravoxel Incoherent Motion (IVIM) Analysis of Diffusion-Weighted Imaging for Prediction of Tumor Size Changes and Imaging Response in Breast Cancer Liver Metastases Undergoing Radioembolization: A Retrospective Single Center Analysis. Medicine (Baltimore) 2016;95:e3275.
65. Menezes-Reis R, Salmon CE, Bonugli GP, Mazoroski D, Tamashiro MH, Savarese LG, Nogueira-Barbosa MH. Lumbar intervertebral discs T2 relaxometry and T1ρ relaxometry correlation with age in asymptomatic young adults. Quant Imaging Med Surg 2016;6:402-12.
66. Wang YX, Zhao F, Griffith JF, Mok GS, Leung JC, Ahuja AT, Yuan J. T1rho and T2 relaxation times for lumbar disc degeneration: an in vivo comparative study at 3.0-Tesla MRI. Eur Radiol 2013;23:228-34.
67. Klauss M, Mayer P, Maier-Hein K, Laun FB, Mehrabi A, Kauczor HU, Stieltjes B. IVIM-diffusion-MRI for the differentiation of solid benign and malign hypervascular liver lesions-Evaluation with two different MR scanners. Eur J Radiol 2016;85:1289-94.

Cite this article as: Li YT, Cercueil JP, Yuan J, Chen W, Loffroy R, Wáng YX. Liver intravoxel incoherent motion (IVIM) magnetic resonance imaging: a comprehensive review of published data on normal values and applications for fibrosis and tumor evaluation. Quant Imaging Med Surg 2017;7(1):59-78. doi: 10.21037/qims.2017.02.03

Table S1 Dslow, PF, Dfast value and measurement information of animal IVIM liver studies*

Paper	Animal	Sample size (n)	Field strength (T)	Respiratory compensation	b value number	b distribution	Post-processing algorithm	Mean Dslow (10^{-3} mm^2/s)	Mean PF (%)	Mean Dfast (10^{-3} mm^2/s)
Eberhardt *et al.* 2016	Rat	21	4.7	Respiratory trigger	9	0, 13, 24, 55, 107, 260, 514, 767, 1020	ROI analysis and asymptotic fitting	1.15±0.14	14.77±6.15	50.28±33.21
Hu *et al*. 2015	Rat	15	3.0	FB	8	0, 25, 50, 100, 150, 300, 500, 800	Pixel-wise asymptotic fitting then ROI analysis with parametric map	0.98±0.07	22.00±3.00	34.99±2.21
Joo *et al*. 2014	Rabbit	6	3.0	FB	7	0, 50, 100, 150, 200, 400, 800	Pixel-wise nonlinear simultaneous fitting then ROI	0.81	16.50	24.70
Chow *et al*. 2012	Rabbit	12	7.0	Respiratory trigger	8	0, 50, 100, 200, 500, 1000, 1500, 2000	ROI analysis then nonlinear simultaneous fitting	0.67±0.08	–	27.24±6.34
Ye *et al*. 2015	Rabbit	8	1.5	FB	12	0, 10, 20, 30, 40, 50, 75, 100, 150, 300, 500, 800	Pixel-wise nonlinear simultaneous fitting then ROI analysis	1.14±0.07	14.60±3.60	143.3±39.3

*, only measurements of normal liver tissue were included. IVIM, intravoxel incoherent motion, FB, free-breathing.